Femtosecond Multicolor Pump−Probe Study of Ultrafast Electron Transfer of $[(NH_3)_5Ru^{III}NCRu^{II}(CN)_5]^-$ in Aqueous Solution

Dong Hee Son, Patanjali Kambhampati, Tak W. Kee, and Paul F. Barbara*

Department of Chemistry and Biochemistry, University of Texas, Austin, Texas 78712

Received: November 13, 2001; In Final Form: January 28, 2002

Femtosecond multicolor pump−probe spectroscopy on the prototypical intramolecular electron-transfer compound ($[(NH_3)_5RuNCRu(CN)_5]^-$; RuRu) in aqueous solution is reported for the first time with sufficient time resolution and spectral coverage to monitor the complete spectral dynamics. From the dynamic absorption spectrum, constructed from the pump−probe data obtained over a wide range of probe wavelengths (570−1300 nm), accurate measurement of the electron transfer (ET) time ($1/k_{ET}$) have been obtained by a global analysis of the data. The data have lead to new insights on the role of solvent and solute nuclear motions in the ET process. Additionally, pump−probe experiments with variable wavelength pump pulses have revealed the presence of a pump wavelength-dependent dynamic feature at early time, which has been assigned to stimulated emission from nonequilibrium excited states.

I. Introduction

Ultrafast spectroscopy of barrierless photochemical reaction in solution offers a unique opportunity to time resolve the reactive trajectory of a solute/solvent system and, as a result, directly time resolve the intramolecular and intermolecular coherent nuclear motions and subsequent relaxations associated with the reaction. This has been particularly valuable in the investigation of photoinduced intramolecular electron transfer (ET) reactions, for which there is considerable experimental and theoretical interest in how the ET reactions are coupled to the solute and solvent nuclear degrees of freedoms, especially in the case of aqueous solutions.[1−3] A key prototype for such investigations is metal−metal charge transfer (MMCT) in mixed valence compounds (eq 1).

$$(NH_3)_5Ru^{III}NCRu^{II}(CN)_5^- \underset{\text{back ET}}{\overset{h\nu}{\rightleftharpoons}} (NH_3)_5Ru^{II}NCRu^{III}(CN)_5^- \quad (1)$$

In MMCT, the photoinduced forward electron transfer between the two metal centers is strongly coupled to both solvent and solute nuclear motions. This produces a large displacement of the coordinates of the coupled modes, which also influences the dynamics of the back ET occurring via internal conversion.[4,5] Recent theoretical and experimental studies of ET reactions in mixed-valence compounds and other intramolecular ET systems have focused on the role of solvent and intramolecular vibrational dynamics on the ET kinetics.[6−9] Analysis of the spectroscopic (static absorption and resonance Raman) data and experimental kinetic measurements demonstrated that ET rates in MMCT systems are influenced by the participation of intramolecular vibrational modes or ultrafast inertial solvation as the promoting mode of the ET process. Experimentally estimated ET rate constants (k_{ET}) have been observed to be in reasonable agreement with the predictions from ET rate theories based on the hybrid model proposed by Barbara and coworkers,[6] which combines Marcus theory and the vibronic theory of Jortner and Bixon.[10−13] Although these studies have provided important insight into the role of various coupled degrees of freedom in determining the ET kinetics, much of the dynamics were not explored due to the limited time resolution and spectral window of the experiment. More recently, we have reported[14] a multicolor pump−probe study of ET in a ruthenium mixed-valence compound ($(NH_3)_5RuNCRu(CN)_5^-$; RuRu) in formamide, ethylene glycol, and glycerol with ∼40 fs time resolution.

In the present paper, we report a detailed multicolor pump−probe study of RuRu in H_2O and D_2O. The results lead to a new, more rigorous spectroscopic measurement of the dynamics of ultrafast ET and subsequent solvent and vibrational relaxation of RuRu in aqueous solution. The dynamic absorption spectrum constructed from the pump−probe transient absorption data over a broad range of probe wavelengths with a high time resolution enables (i) measurement of the back ET times ($1/k_{ET,}$ τ_{ET}), (ii) observation of the dynamics of ground state relaxation after ET, and (iii) identification of vibrational wave packet motion which give rise to non-Condon contributions to the charge transfer absorption. This furthermore offers a detailed qualitative picture of the reaction trajectory of photoinduced ET in RuRu. Finally, the dynamic absorption spectrum is observed to be surprisingly dependent on the pump wavelength. This suggests that stimulated emission from a vibrationally unrelaxed excited state of RuRu is a significant feature in the pump−probe spectroscopy of this compound.

II. Experimental Section

The laser system used for the pump−probe experiment is composed of a home-built Kerr lens mode locked Ti:sapphire oscillator pumped by a Nd:YVO_4 laser and a Ti:sapphire multipass amplifier pumped by a Nd:YLF laser. A detailed description of the laser system can be found elsewhere.[15] Briefly, <20 fs pulses centered at 800 nm and generated from the oscillator were subsequently stretched and amplified to give <35 fs, 0.4 mJ pulses at 1 kHz after compression. The amplified femtosecond laser beam was divided into three beams. The first beam was used to pump an optical parametric amplifier (OPA),

* E-mail: p.barbara@mail.utexas.edu.

10.1021/jp014151f CCC: $22.00
Published on Web 04/12/2002

TABLE 1: Multiexponential Fitting Parameters for the Pump−Probe Transient Absorption Data of RuRu in H_2O and D_2O[a]

solvent	λ_{probe}	$\tau_{1/}$	A_1	τ_2	A_2	τ_3	A_3
H_2O	1300	40	−0.68	150	0.32		
	1200	57 ± 6	−0.60	110 ± 10	0.4		
	1000	67 ± 4	−0.93[b]	80 ± 7		1120 ± 115	0.07
	925	80 ± 3	−0.85[b]	92 ± 6		1140 ± 100	0.15
	800[c]	85 ± 10	−0.85	880 ± 160	0.15		
	685	125	−0.95	1820	−0.05		
	625	130 ± 5	−0.85	1950 ± 200	−0.15		
	600	140 ± 10	−0.80	1980 ± 200	−0.20		
	570	150 ± 5	−0.78	2200 ± 500	−0.22		
D_2O	1300	40	−0.77	225	0.23		
	1200	45	−0.75	230	0.25		
	1000	74 ± 6	−0.88[b]	91 ± 12		1160 ± 10	0.12
	925	84 ± 10	−0.87[b]	144 ± 20		1400 ± 300	0.13
	685	170 ± 8	>0.9	>5000	<0.1		
	625	220 ± 10	>0.9	>5000	<0.1		
	600	210 ± 10	−0.80	3000 ± 1000	−0.20		
	570	210 ± 5	−0.75	3000 ± 1000	−0.25		

[a] Fitting function is $\Sigma A_n \exp(-t/\tau_n)$, and the amplitudes are normalized such that $\Sigma |A_n| = 1$. [b] Amplitude is the sum of two amplitudes A_1 and A_2 having the negative and positive amplitude, respectively. [c] Taken from Reid et al.[7]

which was used to generate variable wavelength pump or probe pulses. The pulses out of the OPA were compressed with an external fused silica prism pair to generate pulses of <25 fs duration. The second beam was used for pumping the sample at 800 nm. The third beam was used to generate white light continuum in a sapphire crystal which was used as the probe. The continuum was also compressed with a fused silica prism pair and the probe wavelength component was preselected before the sample. The compressed continuum pulses typically gave a pump−probe cross-correlation time of 30−45 fs. Throughout the experiment, the cross-correlation time was maintained at 40 fs at all the pump and probe wavelengths.

RuRu was generously supplied by Hupp and co-workers, who synthesized and purified the sample by a previously described procedure.[5,16] The sample solutions of RuRu were rotated, in a 1 mm path length rotating liquid cell with 200 μm thick fused silica windows, to avoid unwanted thermal effects from heating of the sample by the pump pulse. The probe pulse energy was on the order of 1 nJ while the pump pulse was typically 10 μJ. The probe and pump beam waists (fwhm) were 50 and 300 μm, respectively. The polarization of the pump beam was set at magic angle relative to the probe, while the pump−probe crossing angle was 5° at the sample position. To ensure that the transient absorption measurement was made in the linear regime of the photodepletion of the ground-state population, the pump pulse energy was maintained low enough so that less than 5% of the ground-state population was promoted to the excited state by the pump pulse. The transmitted probe beam was detected with Si or InSb photodiodes and the signals were processed with boxcar integrators. All the pump−probe data reported herein are corrected for a signal from the solvent by subtracting the neat solvent signal, properly scaled to the pump intensity, from the pump−probe signal of RuRu in solution.

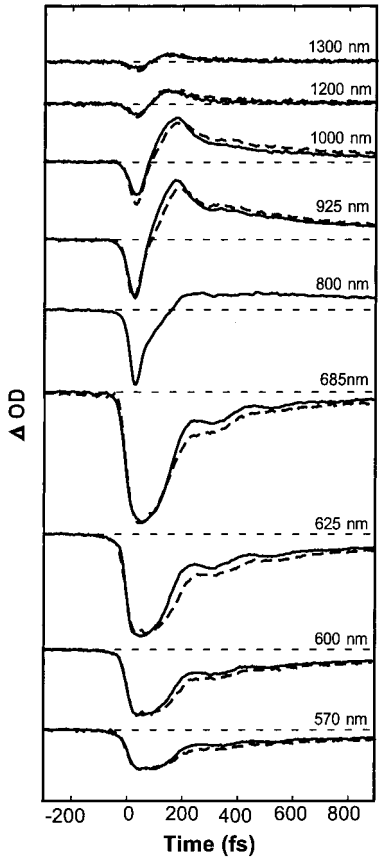

Figure 1. Pump−probe data of RuRu in H_2O (solid line) and D_2O (dashed line) obtained with 800 nm pump and variable wavelength probe. Probe wavelengths are indicated next to each pump−probe data. The 800 nm probe data is taken from Reid et al.[7]

III. Results and Discussions

Overview of the Pump−Probe Data. Comprehensive pump−probe transient absorption data (ΔOD(t)) of RuRu in H_2O (solid line) and D_2O (dashed line) obtained with 800 nm pump and variable wavelength probe are shown in Figure 1. Each ΔOD-(t) pump−probe trace has have been fitted to a multiexponential function, and the fitting parameters are summarized in Table 1. At the probe wavelengths on the blue side of the static absorption spectrum (570−685 nm), the data show an initial instrument response-limited bleach (negative ΔOD) induced by the pump pulse, followed by a recovery of the bleach on multiple time scales (~140 fs, >1 ps). In contrast, at probe wavelengths on the red side of the static absorption spectrum (800−1300 nm), the initial bleach is followed by a net absorption (positive ΔOD). The absorptive signal peaks ca. 200 fs and decays to zero on multiple time scales (~100 fs, >1ps). These features are well described by the ground-state population recovery and the spectral evolution of the nonequilibrium ground-state absorption. The dynamics are independent of the pump intensity even when saturation of the population depletion is observed at high pump intensity. Oscillatory features due to the vibrational

coherence are observed at various probe wavelengths in the pump−probe data.

The recovery of the initial bleach and the decay of the net absorption are slower in D_2O at times earlier than 300 fs. At later times, the dynamics are insensitive to isotopic substitution of the solvent. Since the static absorption spectra of RuRu in both solvents are identical, the differences presented in Figure 1 reflect differences in the actual dynamics upon isotopic substitution of the solvent.

Determination of the ET and Ground-State Relaxation Times. As a starting point of for the analysis, it is informative to consider a simple photodynamical model for internal conversion (i.e., ET) and subsequent ground-state relaxation of RuRu. The model assumes first-order kinetics for the ET reaction, which converts the excited electronic state to the ground state with a time constant of τ_{ET}. It further includes relaxation on the ground state with two exponential decay times (τ_{relax}) in order to account for the spectral shift on the ground state after ET. The experimental ΔOD data are globally fit to the following equation,

$$\Delta OD(\nu,t) = \text{constant} \cdot [(P_{ground}(t) - 1)\sigma_{ground}(\nu) + P_{hot}(t)\sigma_{hot}(\nu,t)]\nu \quad (2)$$

$$\sigma_{hot}(\nu,t) = \sigma_{ground}(\nu + \nu_0(t))$$

$$\nu_0(t) = \nu_0(0)\sum_i a_i \cdot \exp(-t/\tau_{relax,i})$$

where $P_{ground}(t)$ and $P_{hot}(t)$ are the time-dependent population of the equilibrium ground state and nonequilibrium hot ground state, respectively. $\sigma_{ground}(\nu)$ and $\sigma_{hot}(\nu,t)$ are the absorption line shapes of the corresponding states. The time-dependent populations are obtained by solving a set of kinetic equations, where the excitation by a pump pulse of a finite pulse width is treated by using time-dependent pump pulse energy density $W(t)$.

$$\frac{dP_{ground}}{dt} = -BW(t)P_{ground}$$

$$\frac{dP_{excited}}{dt} = BW(t)P_{ground} - \tau_{ET}P_{excited} \quad (3)$$

$$B = \text{Einstein coefficient}$$

$$\frac{dP_{hot}}{dt} = \tau_{ET}P_{excited}$$

$\sigma_{ground}(\nu)$ is the experimental absorption line shape which was determined by fitting the equilibrium absorption spectrum to a log-normal function. $\nu_0(t)$ represents the multiexponential spectral shift of the nonequilibrium ground state. The oscillatory part of the data arising from the vibrational coherence is not considered in this kinetic model. Figure 2 shows the pump−probe data of RuRu in H_2O (solid line) and the result of the global fit (dashed line) to the model. The optimized kinetic parameters from the fit are 80 fs for τ_{ET} and 100 and 600 fs for the ground-state relaxation times τ_{relax}. The other best-fit parameter of the fit are as follows: $a_1 = 0.8$, $a_2 = 0.2$, and $\nu_0 = 5000\ cm^{-1}$. While the model reproduces the dynamics at all probe wavelengths qualitatively, discrepancies are observed at early times in the data with near-IR probe. This may be partly due to the inability of the model to accurately describe all the dynamic processes involved in the ET of RuRu. For instance, description of the time-dependent nonequilibrium ground-state absorption with a simple redshifted ground-state absorption and exclusion of the stimulated emission from the model might contribute to the discrepancies between the experiment and the fit to the model. Nevertheless, the global fit provides a reasonable estimate of τ_{ET} and the time scales of spectral evolution on the ground state.

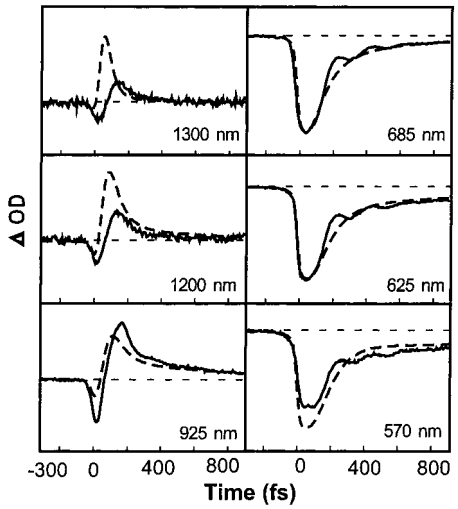

Figure 2. Global fitting of the pump−probe data (RuRu in H_2O) to a kinetic model. The solid line is the experimental data, and the dashed line is the fit to the kinetic model. Model used is described in the text.

A less restrictive analysis of the data was accomplished by the dynamic absorption line shape, $\hat{\sigma}(\nu,t)$ by a different fitting procedure. $\hat{\sigma}(\nu,t)$ was constructed by adding the static absorption spectrum of the ground state population initially excited by the pump pulse, $I_0(\nu)$, to the dynamic ΔOD spectrum, $\Delta OD(\nu,t)$, and correcting for the frequency factor ν (eq 4).

$$\hat{\sigma}(\nu, t) = \frac{\Delta\text{OD}(\nu, t) + I_0(\nu)}{\nu} \quad (4)$$

$\hat{\sigma}(\nu, t)$ calculated in this way represents the absorption from the RuRu molecules excited by the pump pulse. The individual absorption line shape at each time was fit to a log-normal function, and the fitted line shape was used for subsequent analysis. Figure 3a presents the frequency integrated absorption line shape $\sigma(t) = \int\hat{\sigma}(\nu, t)\, d\nu$ at each time. Since $\sigma(t)$ represents the absorption from the RuRu molecules that have returned to the ground electronic state,[17] the rise of $\sigma(t)$ is a direct measure of the ground-state population recovery, which allows the accurate measurement of τ_{ET}.

Interestingly, a negative $\sigma(t)$ is observed zero time, indicating the presence of an "extra" *emission-like* process in the pump−probe data at early times. This can be clearly seen in Figure 4, which compares the static absorption spectrum of RuRu in H_2O and the ΔOD of the pump−probe data near time zero, where it reaches its minimum. If the bleach signal in the pump−probe data originated only from the depletion of the ground-state population, one would expect the envelope of the *time zero* ΔOD to be close to that of the static absorption spectrum. Figure 4 exhibits more negative *time zero* ΔOD near 950 nm than expected from a simple bleach of the static absorption spectrum. We assign this feature to stimulated emission, as discussed in detail below.

Evaluation of τ_{ET} from $\sigma(t)$ was performed by assuming that both the absorption and emission contribute to $\sigma(t)$ with the same exponential rise and decay times, but with the opposite sign of amplitudes. In H_2O, τ_{ET} is determined to be ~100 fs, which is very close to the result from the global fit of the pump−probe data. Figure 3b shows the peak absorption frequency of

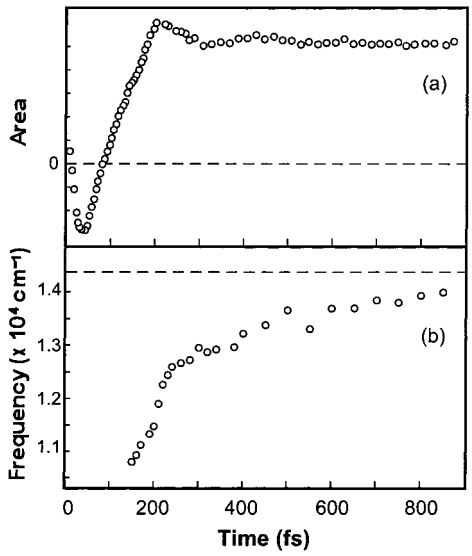

Figure 3. (a) Integrated absorption line shape σ(t) of RuRu in H_2O. Area is calculated from the fitted absorption line shape at each time to a log-normal function. (b) Peak frequency of the absorption line shape for RuRu in H_2O. The horizontal dashed line indicates the frequency at infinite time. The frequency is determined from the fitted absorption line shape.

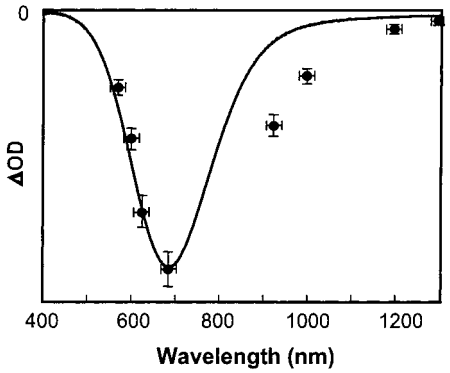

Figure 4. Comparison of the static absorption spectrum and *time zero* ΔOD of RuRu in H_2O.

the nonequilibrium ground state after ET of RuRu in H_2O. The frequency is determined from a log-normal fit of the experimental absorption line shape $\hat{\sigma}(\nu,t)$ at each time. Although reliable absorption frequencies are not available at early times due to interference from stimulated emission, a blueshift of the spectrum toward the equilibrium on two distinct time scales is readily observed. An exponential fit of the data yields two relaxation times of 100 ± 20 and 500 ± 70 fs. These times are consistent with the time scales obtained from the global fit.

The pump−probe data of RuRu in D_2O have been analyzed in the same manner. From the global fit and the analysis of $\sigma(t)$, τ_{ET} is determined to be ~10% longer in D_2O than in H_2O. The dynamics exhibit a varying degree of solvent isotope effect at different time scales as can be seen from the fit parameters in Table 1. The isotope effect is most pronounced for the 100−150 fs (150−220 fs) component in H_2O (D_2O) that corresponds to the bleach recovery at short probe wavelengths (685−570 nm) and decay of net absorption at long probe wavelengths (925−1300 nm). The initial <100 fs recovery of the bleach at long probe wavelengths shows a weaker dependence on the solvent isotope substitution.

ET Kinetics: Comparison to Previous Results and Interpretation. The values of τ_{ET} (80−100 fs in H_2O) obtained in the present study by the two methods are consistent with the previously reported value of 85 fs by Reid et al.[7] using single wavelength pump−probe spectroscopy at 800 nm. The single wavelength pump−probe measurement is, however, more subject to inaccurate evaluation of τ_{ET} due to difficulties in distinguishing population recovery from other relaxation dynamics. This can be seen easily from a distribution of time scales (τ_1 in Table 1) of the early time bleach recovery in individual pump−probe data. The near equivalence of τ_{ET} in the present and previous experiments may be due to the similar absorption coefficient of equilibrium and nonequilibrium ground-state population at 800 nm in H_2O. The solvent isotope effect on τ_{ET} (10%) from the present study, on the other hand, is smaller than that reported (40%) by Reid et al.[7] This discrepancy is not unexpected considering the difficulties in the interpretation of single wavelength pump−probe data discussed above. A larger solvent isotope effect reported in the previous study is likely to be the result of the incomplete separation of the population recovery from the ground state relaxation dynamics which show a large solvent isotope effect at early times (<200 fs).

For ET reactions in solution phase that occur faster than the diffusional solvation time scale, ET is promoted by the high-frequency intramolecular vibrational modes and ultrafast inertial solvation.[2,8,9,18−20] H_2O is known to have a large amplitude ultrafast Gaussian inertial solvation component ($\tau_g = 30-55$ fs), in addition to slower diffusional solvation components ($\tau_d = 120-880$ fs).[21−23] The inertial solvation of water involves the librational motion of water molecules, and its time scale exhibits an isotope effect of 1.4. In the case of RuRu in aqueous solution, the observation of ultrafast ET faster than the average diffusional solvation time scale and the presence of a kinetic solvent isotope effect indicate that ultrafast inertial solvation plays an important role in the ET process.

There is not, however, a direct correlation between ultrafast inertial solvation and the ET process. The fact that τ_{ET} is several times longer than τ_g and that the kinetic solvent isotope effect is weak (10%) raises a question about the exclusive role of ultrafast inertial solvation in determining the ET kinetics. According to dynamic solvent effect theories of electron transfer,[2,6,10,24] in reactions where ET occurs under nonequilibrium conditions, both the solvent relaxation rate and the solvent coordinate dependent microscopic reaction rate determine the rate of the ET reaction in a complex manner. The trajectory along the reaction coordinate is determined by both the solvent and intramolecular vibrational degrees of freedom, which act as the promoting modes. The discrepancy between τ_g and τ_{ET} and the weak solvent kinetic isotope effect observed in RuRu can be explained by the combined role of both ultrafast inertial solvation and intramolecular vibrational modes. In water, the microscopic reaction channels on the solvent coordinate sampled during inertial solvation may not efficiently drive the ET reaction on the time scale of τ_g. This leads to a weakening of the role of inertial solvation in determining the ET kinetics. This may also explain why the solvent isotope effect on τ_{ET} is weaker than observed in τ_g of water. The role of intramolecular vibrational modes in the ET of RuRu is more pronounced in slowly relaxing solvents without inertial solvation component as shown in the previously reported studies.[8,14] In ethylene glycol and glycerol, τ_{ET} of RuRu is ~220 fs and insensitive to the time scales of solvation, which indicates that intramolecular vibrational degrees of freedom plays a major role in ET kinetics for these systems.

Ground-State Energy Disposal. Since RuRu in water has large solvent and vibrational reorganization energies (λ_{sol} = ~4000 cm^{-1}, λ_{vib} = ~2000 cm^{-1}),[25−27] the spectral shift shown in Figure 3b represents, in principle, both vibrational relaxation

and solvation in the ground state. Disentangling the vibrational relaxation dynamics and solvation dynamics is not straightforward in general, since the spectroscopic signatures of both processes are similar in pump−probe spectroscopy. It is interesting to note that two time scales of the spectral shift seen in Figure 3b are similar to the diffusional solvation time of water from transient Stokes shift measurements consistent with an assignment of the dominant contribution of the spectral shift to solvation.[22] The vibrational relaxation time of RuRu was measured for the terminal CN stretching mode in water using infrared spectroscopy. The time scale of the vibrational relaxation of this mode was found to be 0.6−7 ps using 2 ps pulses.[28] In an analogous system where one of the Ru atoms is replaced with Fe, the bridging and terminal CN stretching modes showed relaxation times on the order of picoseconds in D_2O using 200 fs pulses.[29] It is possible, however, that significant portion of the vibrational relaxation occurs also on a similar time scale as solvation RuRu in water, and that this component of vibrational relaxation was not too fast to be resolved by the published infrared spectroscopy experiments (which had a resolution of several hundred femtosecond or longer). It is also possible is that the vibrational excess energy is distributed to Franck−Condon inactive modes and is not observed spectroscopically.

Stimulated Emission and Energy Dependence of the ET Lifetime. The near-zero-time excess negative ΔOD on the red edge of absorption spectrum shown in Figure 4 can be attributed to several processes. In principle, stimulated emission, spectral hole burning, stimulated Stokes Raman, and pump−probe coherent interaction may all contribute to the pump−probe signal as an extra, negative ΔOD. The possibility of pump−probe coherent coupling can be ruled out since the extra, negative signal is observed at probe wavelengths (925−1200 nm) with large detuning from the pump wavelengths (800 nm).[30,31] Furthermore, the recovery of the bleach signal is slower than the instrument response time. Hole burning in the solvent or solute degrees of freedom is unlikely since the RuRu absorption spectrum is substantially broadened by large Franck−Condon activity in a large number of modes.[8] Additionally, the effect of having multiple donor levels (*d*-orbital) split by spin−orbit coupling of ∼1000 cm^{-1} is too small to introduce noticeable selective excitation.[32] We therefore assign the extra, negative ΔOD to stimulated emission.

Figure 5 presents an additional evidence for stimulated emission. At 925 nm probe, the *time zero* ΔOD is significantly reduced when the pump wavelength is changed from 800 to 615 nm. The 685 nm probe data exhibits a small sharp feature near time zero only with 615 nm pump. These observations are consistent with stimulated emission from nonequilibrium excited states. The pump wavelength dependence arises from excess vibrational energy in the excited state. An analogous pump wavelength dependence has been observed for the spontaneous emission in rhodopsin, which was assigned to the emission from vibrationally unrelaxed excited states.[33,34] Theoretical studies have shown that the pump wavelength-dependent behavior of stimulated emission from vibrationally unrelaxed excited states can become more pronounced when the electronic transition is vibrationally coherent as in RuRu.[35] The pump wavelength-dependent stimulated emission disappears faster than the excited-state lifetime of ∼100 fs due to rapid shifting of the emission out of the probe window and partial cancellation of the emission signal by absorption from the relaxing ground state.

In contrast to the strong dependence of stimulated emission on the pump wavelength, no other noticeable pump wavelength dependence is observed in the dynamics. This indicates that the ET kinetics and subsequent relaxation dynamics are not strongly sensitive to the amount of initial excess energy on the excited state. This observation is consistent with a variety of theoretical and experimental results on barrierless inverted regime ET.[3,12]

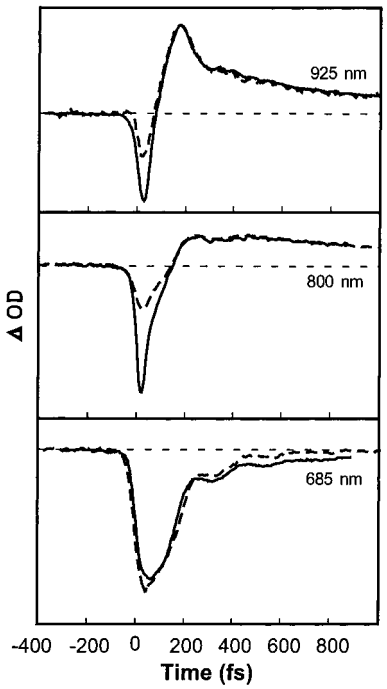

Figure 5. Comparison of the pump−probe data of RuRu in H_2O obtained with 800 (solid line) and 615 nm pump (dashed line). Probe wavelengths are indicated next to each pump−probe data. The 800 nm pump and 800 nm probe data are taken from Reid et al.,[7] which has significant contribution from the coherent artifact.

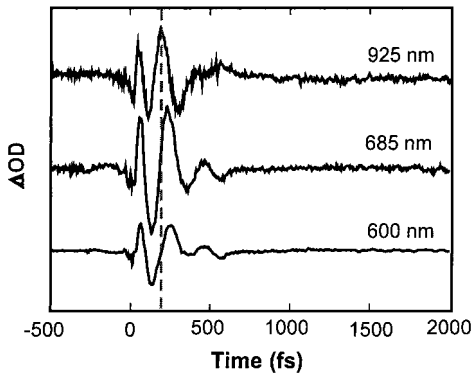

Figure 6. Comparison of the oscillations in the pump−probe data of RuRu in H_2O at different probe wavelengths. Oscillations are isolated from the multiexponential fitting of the pump−probe data. A vertical dashed line is drawn to show the relative phase of oscillation at each probe wavelength.

Vibrational Coherence. Figure 6 shows the oscillatory part of the pump−probe data of RuRu at 600, 685, and 925 nm probe corresponding to the blue, center, and red side of the static absorption spectrum, respectively. A dashed vertical line is drawn to facilitate comparison of the relative phase of the oscillations at each probe wavelength. Oscillations that exist in the pump−probe data indicate the presence of vibrational coherences (vibrational wave packet motion). In principle, vibrational coherence can be generated on both the ground and excited states.[36,37] In RuRu, the vibrational coherence should be primarily on the ground state since the oscillations persist longer (∼300 fs) than the excited-state lifetime (τ_{ET}). Fourier and linear prediction singular value decomposition analysis of

the oscillation show a prominent peak at 160 cm^{-1}. This mode has been observed in the resonance Raman spectrum of RuRu in aqueous solution.[38] Although definitive assignment has not been reached, this mode is probably the vibrational motion of the bond connecting two Ru centers considering that a vibrational mode with a similar frequency observed in a related system was assigned to vibration of the bond connecting a heavy atom donor−acceptor pair.[39] Other higher frequency Raman active modes were reported in previous resonance Raman studies (270, 490, and 580 cm^{-1})[7,40] but are not clearly observed in the present study due to insufficient signal/noise ratio in the pump−probe data. The mechanism of generating ground-state vibrational coherence in RuRu has been assigned to resonant impulsive stimulated Raman scattering (RISRS)[37,41−43] by Reid et al.[7] Impulsive internal conversion of 100 fs, which can efficiently excite up to 160 cm^{-1} mode coherently, was not considered as a possible mechanism based on the observation of high-frequency modes (270, 490, and 580 cm^{-1}) in their study. It has been shown in a recent study by Kambhampati et al. that RISRS is the dominant mechanism in slowly relaxing solvents such as ethylene glycol and glycerol, where the internal conversion is too slow ($\tau_{ET} \approx 220$ fs) for efficient coherent excitation of the observed 160 cm^{-1} mode.[14] These indicate that the active mechanism for the vibrational coherence of RuRu in solution is RISRS. In water, however, the possibility of an additional contribution from impulsive internal conversion for 160 cm^{-1} mode was also proposed.[14]

It is intriguing to observe that the probe wavelength dependence of the phase and amplitude of the oscillation is rather unusual.[44] In RISRS, the amplitude of the oscillation at the center of the ground-state absorption is expected to be minimal since the slope of the absorption line shape determines the amplitude. In contrast, we observe a large oscillation amplitude at the absorption maximum for RuRu in aqueous solution. The phase difference of the oscillation at the blue and red sides of the absorption center is smaller than the expected value of π. Furthermore, oscillatory features are observed in $\sigma(t)$ as shown in Figure 3a. The period of oscillation in $\sigma(t)$ is the same as those observed in the pump−probe data (~200 fs), showing an apparent correlation between the vibrational wave packet motion and the oscillation of $\sigma(t)$. Under the Condon approximation, the frequency-integrated line shape should not exhibit an oscillation, since the electronic transition dipole that determines the oscillator strength is nuclear coordinate independent.[45,46] This suggests that the Condon approximation is inaccurate with respect to the relevant nuclear motions that correspond to the coherently excited vibrational modes. The non-Condon effect that gives rise to modulation of the oscillator strength can also explain the appearance of an intense oscillation at the center of the absorption spectrum and the diminished phase shift in the oscillation. In an intermolecular donor−acceptor complex, oscillatory spontaneous fluorescence has been observed due to a coherently excited intermolecular vibrational mode.[47] The modulation of the oscillator strength for RuRu may be due to wave packet motion of the Ru−Ru separation, which in turn would modulate the donor−acceptor coupling that determines the oscillator strength.[48]

IV. Conclusions

In this paper, we report a detailed investigation on the electron transfer (ET) reaction dynamics of RuRu in aqueous solution using variable wavelength pump−probe spectroscopy. The ET time (τ_{ET}) of RuRu in H_2O is determined to be 80−100 fs and shows ~10% solvent kinetic isotope effect. On the basis of these observations and predictions from the ET kinetic theories, we conclude that both ultrafast inertial solvation and intramolecular vibrational modes promote the ET process of RuRu in water. Following ET, the dynamic spectral evolution of the nonequilibrium ground state is observed, which is assigned to solvation and vibrational relaxation on the ground state. At early times, pump wavelength-dependent stimulated emission from a nonequilibrium excited state is observed. Vibrational coherence on the ground electronic state is observed, which is generated via RISRS mechanism. The unusual probe wavelength dependence of the amplitude and phase of the oscillating wave packet, as well as the oscillating integrated line shape, indicate the presence of non-Condon contribution from the coherently excited vibrational modes.

Acknowledgment. We gratefully acknowledge support of this research by the Basic Energy Sciences Program of the Department of Energy and the Robert A. Welch Foundation.

References and Notes

(1) Barbara, P. F.; Walker, G. C.; Smith, T. P. *Science* **1992**, *256*, 975.
(2) Bagchi, B.; Gayathri, N. *Adv. Chem. Phys.* **1999**, *107*, 1.
(3) Barbara, P. F.; Meyer, T. J.; Ratner, M. A. *J. Phys. Chem.* **1996**, *100*, 13148.
(4) Hupp, J. T.; Meyer, T. J. *Inorg. Chem.* **1987**, *26*, 2332.
(5) Doorn, S. K.; Hupp, J. T. *J. Am. Chem. Soc.* **1989**, *111*, 1142.
(6) Walker, G. C.; Åkesson, E.; Johnson, A. E.; Levinger, N. E.; Barbara, P. F. *J. Phys. Chem.* **1992**, *96*, 3728.
(7) Reid, P. J.; Silva, C.; Barbara, P. F.; Karki, L.; Hupp, J. T. *J. Phys. Chem.* **1995**, *99*, 2609.
(8) Tominaga, K.; Kliner, D. A. V.; Johnson, A. E.; Levinger, N. E.; Barbara, P. F. *J. Chem. Phys.* **1993**, *98*, 1228.
(9) Kliner, D. A. V.; Tominaga, K.; Walker, G. C.; Barbara, P. F. *J. Am. Chem. Soc.* **1992**, *114*, 8323.
(10) Sumi, H.; Marcus, R. A. *J. Chem. Phys.* **1986**, *84*, 4894.
(11) Nadler, W.; Marcus, R. A. *J. Chem. Phys.* **1987**, *86*, 3906.
(12) Bixon, M.; Jortner, J. *Chem. Phys.* **1993**, *176*, 476.
(13) Bixon, M.; Jortner, J.; Verhoeven, J. W. *J. Am. Chem. Soc.* **1994**, *116*, 7349.
(14) Kambhampati, P.; Son, D. H.; Kee, T. W.; Barbara, P. F. *J. Phys. Chem. A* **2000**, *104*, 10637.
(15) Yokoyama, K.; Silva, C.; Son, D.; Walhout, P. K.; Barbara, P. F. *J. Phys. Chem. A* **1998**, *102*, 6957.
(16) Vogler, A.; Kisslinger, J. *J. Am. Chem. Soc.* **1982**, *104*, 2311.
(17) The absence of the excited-state absorption is consistent with the dynamics observed in the pump−probe data and further supported by the absence of pump intensity dependence showing no sequential excitation into higher lying excited states.
(18) Jortner, J.; Bixon, M. *J. Chem. Phys.* **1988**, *88*, 167.
(19) Walker, G. C.; Åkesson, E.; Johnson, A. E.; Levinger, N. E.; Barbara, P. F. *J. Phys. Chem.* **1992**, *96*, 3728.
(20) Yoshihara, K.; Nagasawa, Y.; Yartsev, A.; Kumazaki, S.; Kandori, H.; Johnson, A. E.; Tominaga, K. *J. Photochem. Photobiol. A: Chem.* **1994**, *80*, 169.
(21) Maroncelli, M.; Fleming, G. R. *J. Chem. Phys.* **1988**, *89*, 5044.
(22) Jimenez, R.; Fleming, G. R.; Kumar, P. V.; Maroncelli, M. *Nature* **1994**, *369*, 471.
(23) Lang, M. J.; Jordanides, X. J.; Song, X.; Fleming, G. R. *J. Chem. Phys. A* **1999**, *11*, 5884.
(24) Bixon, B.; Jortner, J. *J. Chem. Phys.* **1988**, *88*, 167.
(25) The reorganization energies were estimated by fitting the static absorption spectrum to the spectral line shape derived from the multimode Brownian oscillator model, along with the vibrational coordinate displacement data obtained from resonance Raman experiments.
(26) Li, B.; Johnson, A. E.; Mukamel, S.; Myers, A. B. *J. Am. Chem. Soc.* **1994**, *116*, 11039.
(27) Walker, G. C.; Barbara, P. F.; Doorn, S. K.; Yuhua, D.; Hupp, J. T. *J. Phys. Chem.* **1991**, *95*, 5712.
(28) Doorn, S. K.; Dyer, R. B.; Stoutland, P. O.; Woodruff, W. H. *J. Am. Chem. Soc.* **1993**, *115*, 6398.
(29) Wang, C.; Mohney, B. K.; Akhremitchev, B. B.; Walker, G. C. *J. Phys. Chem.* **2000**, *104*, 4313.
(30) Eichler, H. J.; Langhans, D.; Massmann, F. *Optics Comm.* **1984**, *50*, 117.
(31) Chachisvilis, M.; Fidder, H.; Sandström, V. *Chem. Phys. Lett.* **1995**, *234*, 141.

(32) Goodman, B. A.; Raynor, J. B. *Adv. Inorg. Chem. Radiochem.* **1970**, *13*, 192.
(33) Kochendoerfer, G. G.; Mathies, R. A. *J. Phys. Chem.* **1996**, *100*, 14526.
(34) Haran, G.; Morlino, E. A.; Matthes, J.; Callender, R. H.; Hochstrasser, R. M. *J. Phys. Chem. A* **1999**, *103*, 2202.
(35) Lin, S. H.; Yeh, C. Y. *Phys. Rev. A* **1990**, *41*, 2718.
(36) Pollard, W. T.; Lee, S.-Y.; Mathies, R. A. *J. Chem. Phys.* **1990**, *92*, 4012.
(37) Pollard, W. T.; Dexheimer, S. L.; Wang, Q.; Peteanu, L. A.; Shank, C. V.; Mathies, R. A. *J. Phys. Chem.* **1992**, *96*, 6147.
(38) Bignozzi, C. A.; Argazzi, R.; Strouse, G. F.; Schoonover, J. R. *Inorg. Chim. Acta* **1998**, *275*, 380.
(39) Dexheimer, S. L.; Pelt, A. D. V.; Brozik, J. A.; Swanson, B. I. *J. Phys. Chem. A* **2000**, *104*, 4308.
(40) Scherer, N. F. personal communication.
(41) Hasche, T.; Ashworth, S. H.; Riedle, E.; Woerner, M.; Elsaesser, T. *Chem. Phys. Lett.* **1995**, *244*, 164.
(42) Bardeen, C. J.; Wang, Q.; Shank, C. V. *J. Phys. Chem. A* **1998**, *102*, 2759.
(43) Ma, Y. Z.; Aschenbrucker, J.; Miller, M.; Gillbro, T. *Chem. Phys. Lett.* **1999**, *300*, 465.
(44) Nelson, K. A.; Ippen, E. P. *Adv. Chem. Phys.* **1989**, *75*, 1.
(45) Pollard, W. T.; Mathies, R. A. *Annu. Rev. Phys. Chem.* **1992**, *43*, 497.
(46) Mazurenko, Y. T.; Smirnov, V. A. *Proceedings of SPIE* **1990**, *1403*, 466.
(47) Rubtsov, I. V.; Yoshihara, K. *J. Phys. Chem.* **1997**, *101*, 6138.
(48) Vance, F. W.; Karki, L.; Reigle, J. K.; Hupp, J. T.; Ratner, M. A. *J. Phys. Chem. A* **1998**, *102*, 8320.